Rolling Shutter Correction in Manhattan World

Pulak Purkait
Toshiba Research Europe
Cambridge, UK
pulak.isi@gmail.com

Christopher Zach
Toshiba Research Europe
Cambridge, UK
christopher.m.zach@gmail.com

Ales Leonardis
University of Birmingham
Birmingham, UK
a.leonardis@cs.bham.ac.uk

Contents

1. Gauge freedom for Joint estimation

In image plane, we estimate the motion parameters $\mathcal{A}$ and the orthogonal VDs $\boldsymbol{\vartheta}$ simultaneously by minimizing the geometric error. *i.e.*,

$$\arg\min_{\boldsymbol{\vartheta},\mathcal{A}} \sum_{i=1}^{N} \min_{\mathcal{E}} \rho\Big(\mathcal{D}([\bar{\mathbf{u}}_i]_\times KR(\boldsymbol{\vartheta})\hat{\mathbf{e}}_j,\ \mathbf{u}_i)\Big) \tag{1}$$

where $\bar{\mathbf{u}}_i = 0.5\mathbf{u}_i + 0.5\mathbf{v}_i$ is the mid-point and $\mathbf{u}_i = KR(\mathbf{r}^u_{\mathcal{A}})^\intercal \mathbf{u}^{rs}_i$ & $\mathbf{v}_i = KR(\mathbf{r}^v_{\mathcal{A}})^\intercal \mathbf{v}^{rs}_i$ are the end points of l_i in GS coordinates. The distance of a point $\mathbf{u}$ from a line $\mathbf{l} = [l_1,\ l_2,\ l_3]^\intercal$ is computed as

$$\mathcal{D}(\mathbf{l},\mathbf{u}) = \mathbf{l}^\intercal\mathbf{u}/\sqrt{l_1^2 + l_2^2}. \tag{2}$$

As discussed in the main paper, the unknown parameters $\boldsymbol{\vartheta}$ and $\mathcal{A}$ are highly dependent on each other in (1). Thus, the natural representation over-parameterize the problem. In general, the gemetric error (1) (and also the other types of error discussed in the main paper) are rather bilinear functions. In following, we investigate the gauge freedom for bilinear functions and then derive the case of joint estimation of the VDS and the motion estimation.

1.1. Bilinear functions

First, consider a bilinear fuction $f(x,y) = x^\intercal y$. We have

$$\partial f = \begin{pmatrix} y^\intercal \\ x^\intercal \end{pmatrix} \qquad\qquad H_f = \begin{pmatrix} \mathbf{0} & \mathbf{I} \\ \mathbf{I} & \mathbf{0} \end{pmatrix},$$

and therefore the second-order Taylor expansion is

$$\begin{aligned} f(x+dx, y+dy) &\approx f(x,y) + \frac{1}{2}\begin{pmatrix} dx \\ dy \end{pmatrix}^\intercal \begin{pmatrix} \mathbf{0} & \mathbf{I} \\ \mathbf{I} & \mathbf{0} \end{pmatrix} \begin{pmatrix} dx \\ dy \end{pmatrix} + \begin{pmatrix} y^\intercal \\ x^\intercal \end{pmatrix} \begin{pmatrix} dx \\ dy \end{pmatrix} \\ &= f(x,y) + dx^\intercal dy + y^\intercal dx + x^\intercal dy. \end{aligned}$$

Note that H_f has full rank, but its eigenvalues are $(1, \ldots, 1, -1, \ldots, -1)$. On the other hand we know that $f(x,y) = x^\intercal y = x^\intercal H H^{-1} y = (H^\intercal x)^\intercal H^{-1} y$. If we choose $dx = H^\intercal x - x = (H^\intercal - I)x$ and $dy = H^{-1}y - y = (H^{-1} - I)y$, then we read

$$\begin{aligned} dx^\intercal dy + y^\intercal dx + x^\intercal dy &= x^\intercal (H^\intercal - I)^\intercal (H^{-1} - I)y + y^\intercal (H^\intercal - I)x + x^\intercal (H^{-1} - I)y \\ &= x^\intercal (I - H - H^{-1} + I)y + x^\intercal (H - I)y + x^\intercal (H^{-1} - I)y \\ &= x^\intercal (2I - H - H^{-1} + H - I + H^{-1} - I)y = 0. \end{aligned}$$

Further, if $dx = (H^\intercal - I)x$ is given, then we obtain constraints on dy,

$$\begin{aligned} 0 &= dx^\intercal dy + y^\intercal dx + x^\intercal dy = x^\intercal (H - I)dy + x^\intercal (H - I)y + x^\intercal dy \\ &= x^\intercal (Hdy - dy + Hy - y + dy) = x^\intercal (Hdy + Hy - y). \end{aligned}$$

A sufficient condition for the above to hold is that $Hdy + Hy - y = 0$ or $dy = H^{-1}(y - Hy) = H^{-1}y - y$, which means that $y + dx = H^{-1}y$ as before.

Now let $f(x,y) = g(x)^\intercal h(y)$ be a "pseudo"-bilinear function, and $n = \dim(x) = \dim(y)$. We obtain

$$\begin{aligned} \partial_x f &= h(y)^\intercal \partial_x g = h^\intercal g' = \sum_i h_i g_i' \\ \partial_y f &= g(x)^\intercal \partial_y h = g^\intercal h' = \sum_i g_i h_i' \\ \partial_{x^2} f &= \sum_i h_i g_i'' \qquad \partial_{y^2} f = \sum_i g_i h_i'' \qquad \partial_{x,y} f = \sum_i (g_i')^\intercal h_i'. \end{aligned}$$

If we want $f(x+dx, y+dy) = f(x,y)$, then using the second order Taylor expansion we obtain the constraint

$$
\begin{aligned}
0 &= \frac{1}{2}\sum_i \begin{pmatrix} dx \\ dy \end{pmatrix}^{\intercal} \begin{pmatrix} h_i g_i'' & (g_i')^{\intercal} h_i' \\ (h_i')^{\intercal} g_i' & g_i h_i'' \end{pmatrix} \begin{pmatrix} dx \\ dy \end{pmatrix} + \begin{pmatrix} h^{\intercal} g' \\ g^{\intercal} h' \end{pmatrix} \begin{pmatrix} dx \\ dy \end{pmatrix} \\
&= \frac{1}{2}\sum_i \left(h_i dx^{\intercal} g_i'' dx + 2dx^{\intercal} (g_i')^{\intercal} h_i' dy + g_i dy^{\intercal} h_i'' dy \right) + h^{\intercal} g' dx + g^{\intercal} h' dy \\
&= \frac{1}{2}\sum_i h_i dx^{\intercal} g_i'' dx + dx^{\intercal} \sum_i \left((g_i')^{\intercal} h_i' dy + g_i' h_i \right) + \frac{1}{2}\sum_i g_i dy^{\intercal} h_i'' dy + g^{\intercal} h' dy \\
&= \frac{1}{2}\sum_i h_i dx^{\intercal} g_i'' dx + \frac{1}{2}\sum_i g_i dy^{\intercal} h_i'' dy + dx^{\intercal} (g')^{\intercal} h' dy + h^{\intercal} g' dx + g^{\intercal} h' dy
\end{aligned}
$$

Now if $dx = H^{\intercal} x - x = (H^{\intercal} - I)x$, we obtain

$$
0 = \frac{1}{2}\sum_i h_i x^{\intercal} (H - I) g_i'' (H^{\intercal} - I) x + x^{\intercal} (H - I) \sum_i \left((g_i')^{\intercal} h_i' dy + g_i' h_i \right) + \frac{1}{2}\sum_i g_i dy^{\intercal} h_i'' dy + g^{\intercal} h' dy
$$

This doesn't seem to go anywhere.

Let us linearize $g(x + dx) \approx g(x) + g' dx$ and $h(y + dy) \approx h(y) + h' dy$, then

$$
f(x + dx, y + dx) \approx (g + g' dx)^{\intercal} (h + h' dy) = f(x, y) + dx^{\intercal} (g')^{\intercal} h + g^{\intercal} h' dy + dx^{\intercal} (g')^{\intercal} h' dy,
$$

i.e. the constraint is

$$
dx^{\intercal} (g')^{\intercal} h + g^{\intercal} h' dy + dx^{\intercal} (g')^{\intercal} h' dy = 0.
$$

Now let $dx = (H^{\intercal} - I)x$, then we obtain

$$
\begin{aligned}
0 &= x^{\intercal} (H - I) (g')^{\intercal} h + g^{\intercal} h' dy + x^{\intercal} (H - I) (g')^{\intercal} h' dy \\
&= x^{\intercal} (H - I) (g')^{\intercal} h + \left(g^{\intercal} h' + x^{\intercal} (H - I) (g')^{\intercal} h' \right) dy.
\end{aligned}
$$

Note that this is only a scalar constraint on dy. Now for every x there exists a matrix A_x (dependent on the current value of x) such that $g(x) = A_x^{\intercal} x$. This yields

$$
0 = x^{\intercal} (H - I) (g')^{\intercal} h + x^{\intercal} \left(A_x h' + (H - I) (g')^{\intercal} h' \right) dy
$$

and sufficient conditions are given by

$$
0 = (H - I) (g')^{\intercal} h + \left(A_x h' + (H - I) (g')^{\intercal} h' \right) dy.
$$

Hence, a particular solution for dy is given by

$$
dy = \left(A_x h' + (H - I) (g')^{\intercal} h' \right)^{-1} (I - H) (g')^{\intercal} h.
$$

If $g = Id$, $h = Id$, then $A_x = I$, $g' = I$, $h' = I$ and

$$
dy = \left(I + (H - I) I \right)^{-1} (I - H) I y = H^{-1} (y - Hy) = H^{-1} y - y
$$

as earlier. Now let $H = I + \varepsilon B$, then

$$
dy = \varepsilon \left(A_x h' + \varepsilon B (g')^{\intercal} h' \right)^{-1} B (g')^{\intercal} h,
$$

and dy scales with the magnitide ε of the update.

What if $g = Id$, $h = Id$ and $dx = (H^\intercal - I)x$, but A_x is chosen arbitrarily such that $g(x) = A_x^\intercal x$? Then

$$dy = \big(A_x + H - I\big)^{-1}(I - H)y$$

and

$$\begin{aligned}(H-I)(g')^\intercal h + \big(A_x h' + (H-I)(g')^\intercal h'\big)dy &= (H-I)y + \big(A_x + H - I\big)\big(A_x + H - I\big)^{-1}(I-H)y \\ &= (H-I)y + (I-H)y = 0.\end{aligned}$$

This means that there are additional degrees of freedom in $f(x, y) = g(x)^\intercal h(y)$ beyond chossing $H \in \mathbb{R}^{m\times m}$ (at an infinitesimal scale). Now

$$(x + dx)^\intercal (y + dy) = x^\intercal H\left(I + \big(A_x + H - I\big)^{-1}(I - H)\right) y \neq x^\intercal y$$

in general (unless $A_x = I$).

1.2. Counting d.o.f.

Let $Q \in \mathbb{R}^{n\times n}$, then there exists an $A \in \mathbb{R}^{m\times m}$ such that $g(Px) = A^\intercal g(x)$. A has $m^2 - n$ d.o.f. Similarly, let $B \in \mathbb{R}^{m\times m}$ such that $h(Qy) = Bh(y)$ for some $n \times n$ matrix Q. B has $m^2 - n$ d.o.f. One has

$$g(Px)^\intercal h(Qy) = g(x)^\intercal AB\, h(y).$$

There is now the extra (scalar) constraint on A and B that $g(x)^\intercal AB\, h(y) = g(x)^\intercal h(y)$. A sufficient condition is $AB = I$, but this may be unnecessarily strong, in particular since A and B may depend on x and y.

1.3. Minimum norm dy

The main constraint after linearizing $g(x + dx)$ and $h(y + dy)$ is given by

$$dx^\intercal (g')^\intercal h + g^\intercal h' dy + dx^\intercal (g')^\intercal h' dy = h^\intercal g' dx + (g + g' dx)^\intercal h' dy = 0.$$

Using the fact that $\arg\min_\xi \|\xi\|^2/2 + \imath\{c^\intercal \xi = d\} = dc/\|c\|^2$, we obtain for a minimal-norm dy

$$dy = \frac{-h^\intercal g' dx}{\big\|(g + g' dx)^\intercal h'\big\|^2}(h')^\intercal (g + g' dx).$$

Note that $g + g'dx$ (the linearization of $g(x + dx)$) may not be in the null space of h'. If we only linearize $h(y + dy) \approx h + h'dy$, the constraint reads as

$$g(x + dx)^\intercal (h + h' dy) - g^\intercal h = 0,$$

leading to

$$dy = \frac{(g - g(x + dx))^\intercal h}{\big\|g(x + dx)^\intercal h'\big\|^2}(h')^\intercal g(x + dx).$$

For $g = Id$, $h = Id$, $h' = I$, $x + dx = H^\intercal x$ we obtain

$$
\begin{aligned}
y + dy = y + \frac{(x - H^\intercal x)^\intercal y}{\|H^\intercal x\|^2} H^\intercal x &= \frac{x^\intercal H H^\intercal x y + y^\intercal x H^\intercal x - y^\intercal H^\intercal x H^\intercal x}{\|H^\intercal x\|^2} \\
&= \frac{x^\intercal H H^\intercal x y + H^\intercal x x^\intercal y - H^\intercal x x^\intercal H y}{\|H^\intercal x\|^2} \\
&= \frac{x^\intercal H H^\intercal x I + H^\intercal x x^\intercal - H^\intercal x x^\intercal H}{\|H^\intercal x\|^2} y.
\end{aligned}
$$

For $H = I + \varepsilon B$ we obtain

$$
\begin{aligned}
y + dy &= \frac{x^\intercal (I + \varepsilon B)(I + \varepsilon B)^\intercal x I + (I + \varepsilon B)^\intercal x x^\intercal - (I + \varepsilon B)^\intercal x x^\intercal (I + \varepsilon B)}{\|(I + \varepsilon B)^\intercal x\|^2} y \\
&= \frac{x^\intercal (I + \varepsilon B + \varepsilon B^\intercal + \varepsilon^2 B B^\intercal) x I + (I + \varepsilon B)^\intercal x x^\intercal - x x^\intercal - \varepsilon B^\intercal x x^\intercal - \varepsilon x x^\intercal B - \varepsilon^2 B^\intercal x x^\intercal B}{\|(I + \varepsilon B)^\intercal x\|^2} y \\
&= \frac{x^\intercal (I + \varepsilon B + \varepsilon B^\intercal + \varepsilon^2 B B^\intercal) x I - \varepsilon x x^\intercal B - \varepsilon^2 B^\intercal x x^\intercal B}{\|(I + \varepsilon B)^\intercal x\|^2} y
\end{aligned}
$$

For ε small we have therefore

$$
y + dy \approx \frac{x^\intercal x I + \varepsilon x^\intercal B x I + \varepsilon x^\intercal B^\intercal x I - \varepsilon x x^\intercal B}{\|(I + \varepsilon B)^\intercal x\|^2} y.
$$

Hmmm. Numerical examples indicate that for small ε one has $y + dy \approx H^{-1} y$.

In the infinitesimal setting we have the following result: changing x by an infinitesimal dx leads to an update for y according to

$$
dy = \frac{(g - g(x + dx))^\intercal h}{\|g(x + dx)^\intercal h'\|^2} (h')^\intercal g(x + dx) = \frac{-h^\intercal g' dx}{\|(g + g' dx)^\intercal h'\|^2} (h')^\intercal (g + g' dx),
$$

which is a PDE coupling dx and dy. dy is well-defined as long as $g(x + dx)$ is not in the null space of h' (which means that the local linear model of $h(y)$ must be able to “interact” with the value $g(x + dx)$). A sufficient conditions is that h' has full rank.

Now let $x(t)$, $t \in [0, 1]$ evolve to reach Hx from a given starting point x, e.g. $x(t) = (1 - t)x + tHx$ and $dx(t) = \dot{x}(t)dt = (Hx - x)dt$. We have (using $\Delta x = \varepsilon \dot{x}(t)$)

$$
\Delta y(t) = y(t + \varepsilon) - y(t) = \frac{-\varepsilon h^\intercal g' \dot{x}(t)}{\|(g + \varepsilon g' \dot{x}(t))^\intercal h'\|^2} (h')^\intercal (g + \varepsilon g' \dot{x}(t)) =: F_t(\varepsilon)
$$

and therefore

$$
\dot{y}(t) = \lim_{\varepsilon \to 0} \frac{y(t + \varepsilon) - y(t)}{\varepsilon} = \lim_{\varepsilon \to 0} \frac{F_t(\varepsilon)}{\varepsilon} = F_t'.
$$

Finally the values for $y(1)$ can be found by integration,

$$
y(1) = \int_{t=0}^{1} \dot{y}(t) dt.
$$

1.4. How does this apply to Manhattan-world rolling shutter compensation?

For the error in the image plane, the cost function can be abstractly written as $\mathbf{g}(\omega_v)^\intercal \mathbf{h}(\omega_{RS})$, where ω_v and ω_{RS} is a minimal 3-dimensional parametrization of rotation matrices. Each term $g_i(\omega_v)^\intercal h_i(\omega_{RS})$ is the squared point-line distance between the vanishing point v and the motion compensated line endpoints s, t:

$$v_i = \pi(R(\omega_v)e_{j_i}) \qquad s_i = \pi(R(\omega_{RS})\hat{s}_i) \qquad t_i = \pi(R(\omega_{RS})\hat{t}_i)$$
$$d^2(v_i, s_i \times t_i) = \frac{(v_i^\intercal(s_i \times t_i))^2}{\|(s_i \times t_i)_{1,2}\|^2} = \left(v_i^\intercal \frac{s_i \times t_i}{\|(s_i \times t_i)_{1,2}\|}\right)^2.$$

Since the line normal is normalized, we also can drop the projection π and replace $s_i \times t_i$ by $(R(\omega_{RS})\hat{s}_i) \times (R(\omega_{RS})\hat{t}_i)$.

We further need the observation that for two vectors u and v it holds

$$(u^\intercal v)^2 = (\sum_i u_i v_i)^2 = \sum_{i,j} u_i u_j v_i v_j = \operatorname{vec}(u \otimes u)^\intercal \operatorname{vec}(v \otimes v),$$

i.e. a squared inner product can be written as dot product in a non-linearly transformed higher-dimensional space.

In this setting

$$g(\omega_v) = \operatorname{vec}(a \otimes a) \qquad a_i = \pi(R(\omega_v)e_{j(i)})$$
$$h(\omega_{RS}) = \operatorname{vec}(b \otimes b) \qquad b_i = \frac{(R(\omega_{RS})\hat{s}_i) \times (R(\omega_{RS})\hat{t}_i)}{\left\|(R(\omega_{RS})\hat{s}_i) \times (R(\omega_{RS}\hat{t}_i))\right\|_{1,2}}$$

and $h', g' \in \mathbb{R}^{4N \times 3}$, where N is the number of line segments. Since $4N \gg 3$, h' will be most likely of full rank.

2. Optimization of the non-linear objective

We employ the Levenberg-Marquardt algorithm to optimize (1). To avoid sub-gradients, we replace non-smooth $\min$ operator by a smooth $\operatorname{softmin}$ operator

$$\operatorname{softmin}_{j\in\mathcal{E}}(z_j;\ \sigma) = -\sigma \log\Big(\sum_{j\in\mathcal{E}} \exp(-z_j/\sigma)\Big). \tag{3}$$

where σ is chosen as 0.0025. The gradient of $\operatorname{softmin}$ maps $\{z_j\}_{j\in\mathcal{E}}$ in the range $(0,\ 1)$ that add up to 1.

2.1. Computation of the Jacobian

The Jacobian $\mathcal{J}_{\mathcal{A},\,\boldsymbol{\vartheta}}$ of $\mathcal{D}([\mathbf{v}_i]_\times KR(\boldsymbol{\vartheta})\hat{\mathbf{e}},\ \mathbf{u}_i)$ is evaluated at $(\mathcal{A}^k,\ \boldsymbol{\vartheta}^k)$ and is carried out by applying the chain rule as follows:

$$\mathcal{J}_{\mathcal{A},\,\boldsymbol{\vartheta}} = \begin{bmatrix} \frac{\partial \mathcal{D}([\mathbf{v}_i]_\times KR(\boldsymbol{\vartheta})\hat{\mathbf{e}},\, \mathbf{u}_i)}{\partial \mathcal{A}} \\ \frac{\partial \mathcal{D}([\mathbf{v}_i]_\times KR(\boldsymbol{\vartheta})\hat{\mathbf{e}},\, \mathbf{u}_i)}{\partial \boldsymbol{\vartheta}} \end{bmatrix}, \tag{4}$$

$$\begin{aligned} \frac{\partial \mathcal{D}}{\partial \mathcal{A}} &\approx \mathbf{u}_i^\intercal (R(\boldsymbol{\vartheta})\hat{\mathbf{e}})^\intercal \frac{\partial [\mathbf{v}_i]_\times}{\partial \mathcal{A}} + ([\mathbf{v}_i]_\times KR(\boldsymbol{\vartheta})\hat{\mathbf{e}})^\intercal \frac{\partial \mathbf{u}_i}{\partial \mathcal{A}}, \\ \frac{\partial \mathcal{D}}{\partial \boldsymbol{\vartheta}} &\approx \mathbf{u}_i^\intercal [\mathbf{v}_i]_\times K \frac{\partial R(\boldsymbol{\vartheta})\hat{\mathbf{e}}}{\partial \boldsymbol{\vartheta}}. \end{aligned} \tag{5}$$

Substituting, $\mathbf{u}_i = KR(\mathbf{r}^u_{\mathcal{A}})^\intercal \mathbf{u}^{rs}_i \quad \& \quad \mathbf{v}_i = KR(\mathbf{r}^v_{\mathcal{A}})^\intercal \mathbf{v}^{rs}_i$

$$\frac{\partial \mathbf{u}_i}{\partial \mathcal{A}} = K\frac{\partial R(\mathbf{r}^u_{\mathcal{A}})^\intercal \mathbf{u}^{rs}_i}{\partial \mathcal{A}}, \ \frac{\partial [\mathbf{v}_i]_\times}{\partial \mathcal{A}} = \left[K\frac{\partial R(\mathbf{r}^v_{\mathcal{A}})^\intercal \mathbf{v}^{rs}_i}{\partial \mathcal{A}}\right]_\times . \tag{6}$$

Under the choice of ρ ,

$$\rho'(x) = \begin{cases} x & |x| < \delta \\ \delta * sgn(x) & otherwise. \end{cases} \tag{7}$$

$$\frac{\partial R(\mathbf{r}^u_{\mathcal{A}})^\intercal \mathbf{u}^{rs}_i}{\partial \mathbf{r}_{\mathcal{A}}} \approx \frac{\partial}{\partial \mathbf{r}_{\mathcal{A}}}\left[\ \cdot\ \right]\mathbf{u}^{rs}_i - R(\mathbf{r}^u_{\mathcal{A}})^\intercal \mathbf{u}^{rs}_i \begin{bmatrix} r_x \\ r_y \\ r_z \end{bmatrix} \tag{8}$$

$$\frac{\partial}{\partial \mathbf{r}_{\mathcal{A}}}\left[\ \cdot\ \right]\mathbf{u}^{rs}_i = 2 \times \begin{bmatrix} [r_x, & r_y, & r_z] \cdot \mathbf{u}^{rs}_i & [-r_y, & r_x, & -1] \cdot \mathbf{u}^{rs}_i & [-r_z, & 1, & r_x] \cdot \mathbf{u}^{rs}_i \\ [r_y, & -r_x, & 1] \cdot \mathbf{u}^{rs}_i & [r_x, & r_y, & r_z] \cdot \mathbf{u}^{rs}_i & [-1, & -r_z, & r_y] \cdot \mathbf{u}^{rs}_i \\ [r_z, & -1, & -r_x] \cdot \mathbf{u}^{rs}_i & [1, & r_z, & -r_y] \cdot \mathbf{u}^{rs}_i & [r_x, & r_y, & r_z] \cdot \mathbf{u}^{rs}_i \end{bmatrix}$$

$$\frac{\partial r_{\mathcal{A}}}{\partial \mathcal{A}} = \begin{bmatrix} \mathbf{pn} & \mathbf{0} & \mathbf{0} \\ \mathbf{0} & \mathbf{pn} & \mathbf{0} \\ \mathbf{0} & \mathbf{0} & \mathbf{pn} \end{bmatrix} \tag{9}$$

where $\mathbf{pn} = [1,\ p,\ \ldots,\ p^n]^\intercal$ and $\mathbf{0} = [0,\ 0,\ \ldots,\ 0]$ (n+1 times). $\frac{\partial R(\boldsymbol{\vartheta})\mathbf{u}_j}{\partial \boldsymbol{\vartheta}}$ is computed similarly as (8).

3. Experiments on Additional Datasets

We execute on some other real datasets in addition to the main paper. The results on some of the images are shown in the Figure 1 and 2. Here we consider only 50 point correspondences in Figure 1 and 100 point correspondences in Figure 2 for quantitative evaluations. We experienced similar performance to the multiple frame methods [9, 12] and better than the single frame method [26]. Note that the results of [9, 12] are downloaded from their respective webpages. The authors of [26] shared their results with us.

(a) $|\mathcal{R}_F| = 36.75$, $\sigma_{\mathcal{R}} = 3.51$ [9] (b) $|\mathcal{R}_F| = 29.92$, $\sigma_{\mathcal{R}} = 2.10$ [26] (c) $|\mathcal{R}_F| = 31.45$, $\sigma_{\mathcal{R}} = 1.82$ **ours**

Figure 1: Comparison of the proposed method with [9] and [26] on the image sequences `clipo4.mp4` from [9].

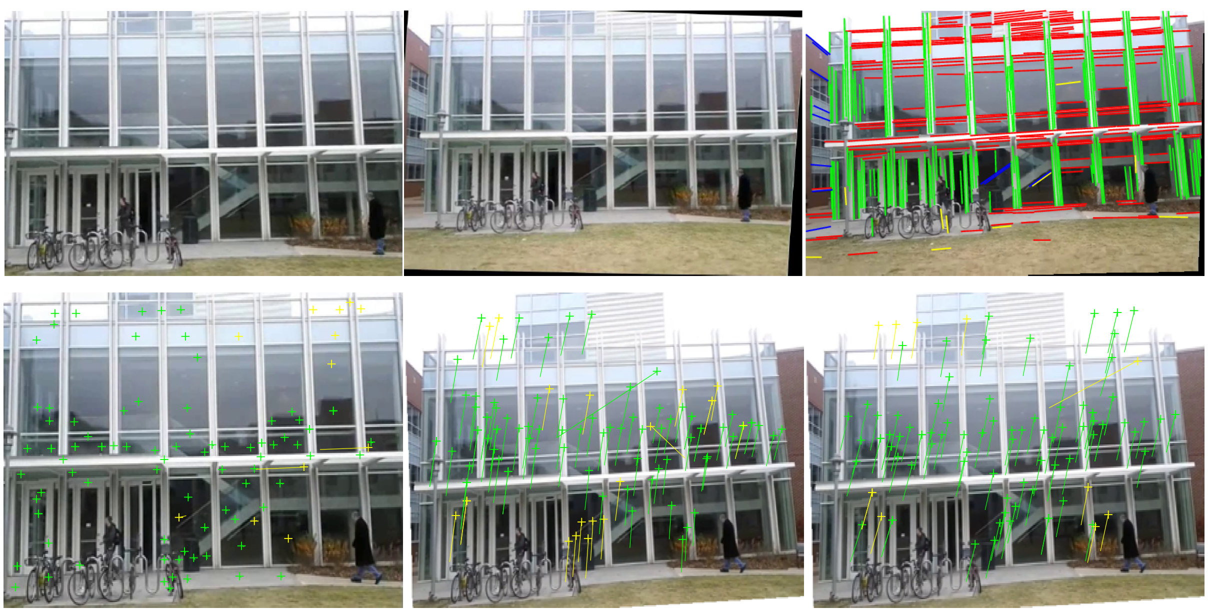

(a) $|\mathcal{R}_F| = 94.45$, $\sigma_{\mathcal{R}} = 3.46$ [12] (b) $|\mathcal{R}_F| = 89.52$, $\sigma_{\mathcal{R}} = 2.95$ [26] (c) $|\mathcal{R}_F| = 94.58$, $\sigma_{\mathcal{R}} = 3.17$ **ours**

Figure 2: Comparison of the proposed method with [12] and [26] on the image sequence `nxs_wobble_2_result_dual.mov` from [12].

References

[1] O. Ait-Aider, N. Andreff, J. M. Lavest, and P. Martinet. Simultaneous object pose and velocity computation using a single view from a rolling shutter camera. In *ECCV*, pages 56–68. Springer, 2006.

[2] C. Albl, Z. Kukelova, and T. Pajdla. R6p-rolling shutter absolute camera pose. In *CVPR*, pages 2292–2300. IEEE Computer Society, 2015.

[3] M. Antunes and J. P. Barreto. A global approach for the detection of vanishing points and mutually orthogonal vanishing directions. In *CVPR*, pages 1336–1343, 2013.

[4] K. S. Arun, T. S. Huang, and S. D. Blostein. Least-squares fitting of two 3-d point sets. *IEEE Transactions on pattern analysis and machine intelligence*, (5):698–700, 1987.

[5] J.-C. Bazin, Y. Seo, C. Demonceaux, P. Vasseur, K. Ikeuchi, I. Kweon, and M. Pollefeys. Globally optimal line clustering and vanishing point estimation in manhattan world. In *CVPR*, pages 638–645. IEEE Computer Society, 2012.

[6] J. M. Coughlan and A. L. Yuille. Manhattan world: Orientation and outlier detection by bayesian inference. *Neural Computation*, 15(5):1063–1088, 2003.

[7] Y. Dai, H. Li, and L. Kneip. Rolling shutter camera relative pose: Generalized epipolar geometry. In *CVPR*. IEEE Computer Society, June 2016.

[8] P. Denis, J. H. Elder, and F. J. Estrada. Efficient edge-based methods for estimating manhattan frames in urban imagery. In *ECCV*, pages 197–210. Springer, 2008.

[9] P.-E. Forssén and E. Ringaby. Rectifying rolling shutter video from hand-held devices. In *CVPR*, pages 507–514. IEEE Computer Society, 2010. 7, 8, 15

[10] G. H. Golub and C. F. Van Loan. *Matrix computations*, volume 3. JHU Press, 2012.

[11] v. G. R. Grompone, J. Jakubowicz, J.-M. Morel, and G. Randall. Lsd: a fast line segment detector with a false detection control. *IEEE TPAMI*, 32(4):722–732, 2010.

[12] M. Grundmann, V. Kwatra, D. Castro, and I. Essa. Calibration-free rolling shutter removal. In *ICCP*, pages 1–8. IEEE Computer Society, 2012. 7, 8, 15

[13] R. Hartley and A. Zisserman. *Multiple view geometry in computer vision*. Cambridge university press, 2003.

[14] S. Hee Park and M. Levoy. Gyro-based multi-image deconvolution for removing handshake blur. In *CVPR*, pages 3366–3373. IEEE Computer Society, 2014.

[15] P. J. Huber. *Robust statistics*. Springer, 2011.

[16] C. Jia and B. L. Evans. Probabilistic 3-d motion estimation for rolling shutter video rectification from visual and inertial measurements. In *MMSP*, 2012. 16

[17] R. Köhler, M. Hirsch, B. Mohler, B. Schölkopf, and S. Harmeling. Recording and playback of camera shake: Benchmarking blind deconvolution with a real-world database. In *ECCV*, pages 27–40. Springer, 2012.

[18] J. Košecká and W. Zhang. Video compass. In *ECCV*, pages 476–490. Springer, 2002.

[19] T. Kroeger, D. Dai, and L. Van Gool. Joint vanishing point extraction and tracking. In *CVPR*, pages 2449–2457. IEEE Computer Society, 2015.

[20] J.-K. Lee and K.-J. Yoon. Real-time joint estimation of camera orientation and vanishing points. In *CVPR*, pages 1866–1874. IEEE Computer Society, 2015.

[21] D. G. Lowe. Distinctive image features from scale-invariant keypoints. *IJCV*, 60(2):91–110, 2004.

[22] P. F. McLauchlan. Gauge independence in optimization algorithms for 3d vision. In *International Workshop on Vision Algorithms*, pages 183–199. Springer, 1999.

[23] F. M. Mirzaei and S. I. Roumeliotis. Optimal estimation of vanishing points in a manhattan world. In *ICCV*, pages 2454–2461. IEEE Computer Society, 2011.

[24] A. Morawiec. *Orientations and rotations*. Springer, 2003.

[25] A. Patron-Perez, S. Lovegrove, and G. Sibley. A spline-based trajectory representation for sensor fusion and rolling shutter cameras. *IJCV*, 113(3):208–219, 2015.

[26] V. Rengarajan, A. N. Rajagopalan, and R. Aravind. From bows to arrows: Rolling shutter rectification of urban scenes. In *CVPR*, pages 2773–2781, 2016. 7, 8, 11, 14, 15, 16

[27] O. Saurer, K. Koser, J.-Y. Bouguet, and M. Pollefeys. Rolling shutter stereo. In *ICCV*, pages 465–472, 2013.

[28] A. Saxena, S. H. Chung, and A. Y. Ng. 3-d depth reconstruction from a single still image. *IJCV*, 76(1):53–69, 2008.

[29] S. Su and W. Heidrich. Rolling shutter motion deblurring. In *CVPR*, pages 1529–1537. IEEE Computer Society, June 2015.

[30] J.-P. Tardif. Non-iterative approach for fast and accurate vanishing point detection. In *ICCV*, pages 1250–1257. IEEE Computer Society, 2009.

[31] R. Toldo and A. Fusiello. Robust multiple structures estimation with j-linkage. In *ECCV*, pages 537–547. Springer, 2008.

[32] E. Tretyak, O. Barinova, P. Kohli, and V. Lempitsky. Geometric image parsing in man-made environments. *IJCV*, 97(3):305–321, 2012.

[33] B. Triggs, P. F. McLauchlan, R. I. Hartley, and A. W. Fitzgibbon. Bundle adjustment–a modern synthesis. In *International workshop on vision algorithms*, pages 298–372. Springer, 1999.

[34] A. Yuille. The manhattan world assumption: Regularities in scene statistics which enable bayesian inference. In *NIPS*, 2000.

[35] M. Zhai, S. Workman, and N. Jacobs. Detecting vanishing points using global image context in a non-manhattan world. In *CVPR*, pages 5657–5665. IEEE Computer Society, June 2016.

[36] L. Zhang, H. Lu, X. Hu, and R. Koch. Vanishing point estimation and line classification in a manhattan world with a unifying camera model. *International Journal of Computer Vision*, 117(2):111–130, 2016.

4. Images from the main paper

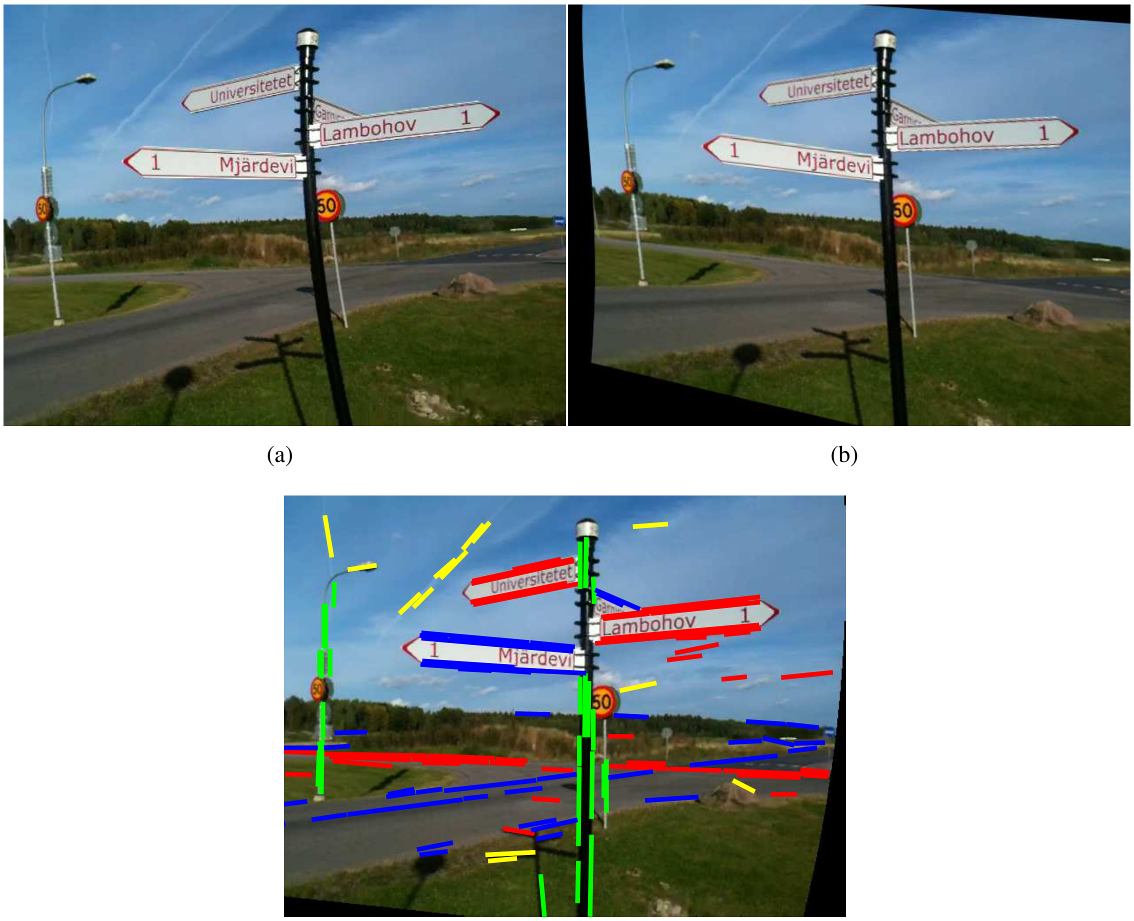

(a) (b) (c)

Figure 3: (a) A real rolling shutter distorted image. (b) Rectified by Rengarajan *et al*. [26]. (c) Proposed simultaneous estimation of orthogonal vanishing directions and rolling shutter motion. The colors *red*, *green* and *blue* are employed for the orthogonal vanishing directions, while *yellow* is used to mark the outliers (lines which are not associated with any of the vanishing directions).

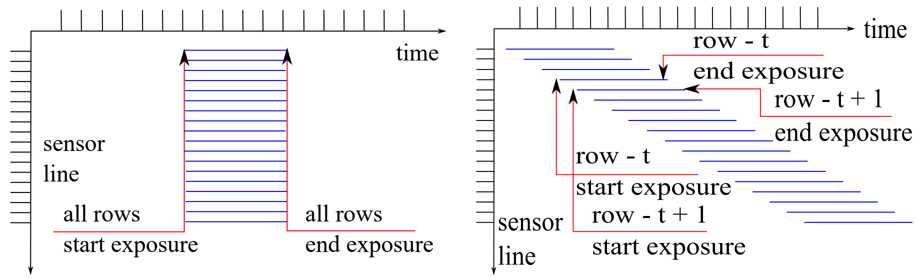

(a) (b)

Figure 4: (a) A global shutter opens to allow light to strike the entire sensor surface all at once. (b) In contrast, a rolling shutter exposes the image line-by-line. Depending on the selected exposure time, distortions can occur when the camera moves during the exposure process—the so-called rolling shutter effects.

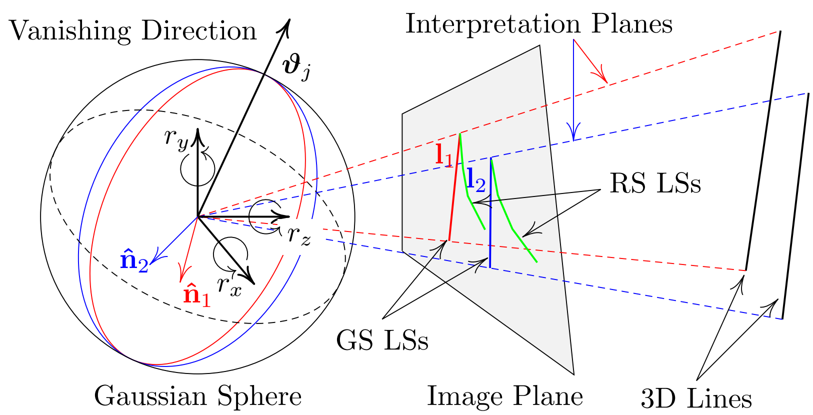

Figure 5: The 3D parallel lines in the world space are projected into the concurrent LSs (green) on a GS camera and arc segments (red) for RS camera.

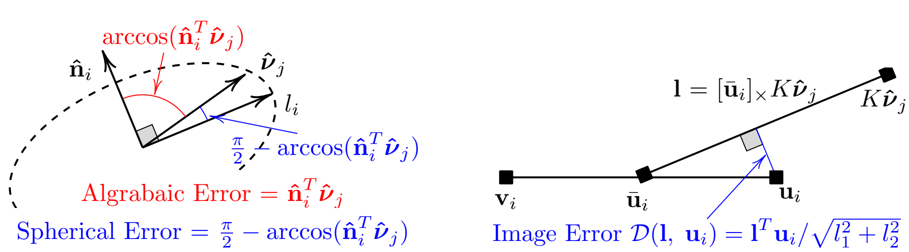

Figure 6: Different choices of errors utilized for joint estimation of vanishing directions and camera motions.

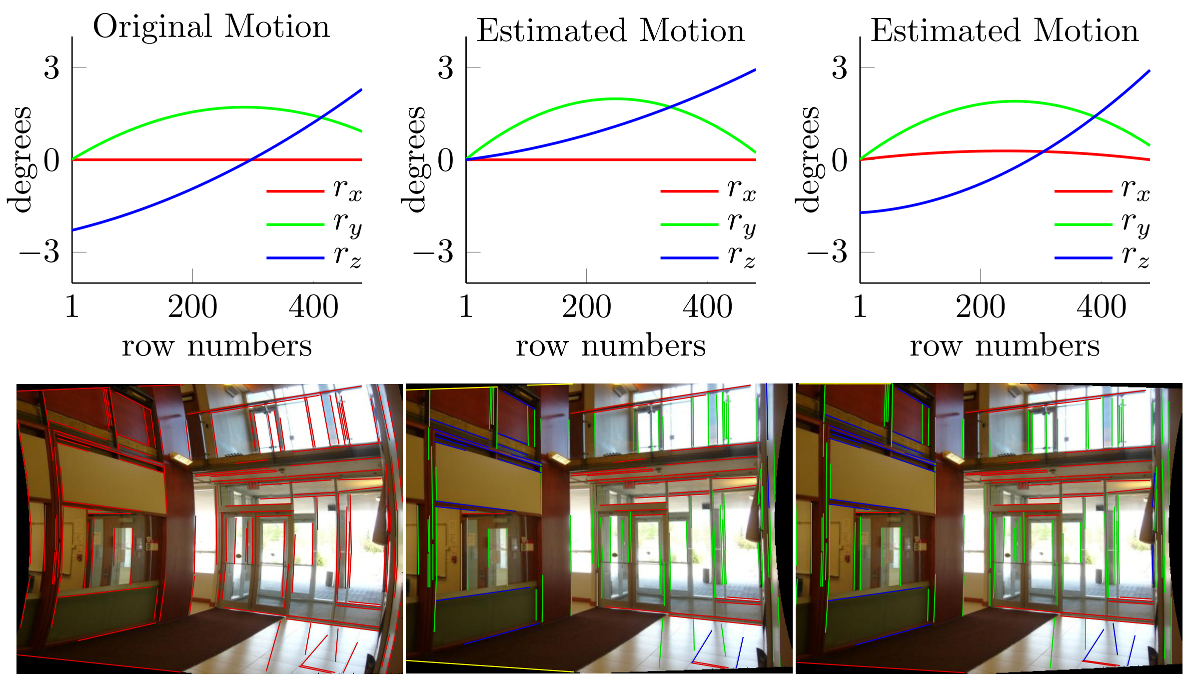

(a) Synthetic Image (b) Natural Choice (c) Aesthetic Choice

Figure 7: Joint estimation of the RS camera motion and the orthogonal VDs: (a) a synthetically generated polynomial motion and the extracted LSs on the synthetic image, (b) joint estimation of RS camera motion and the orthogonal VDs with natural choice of gauge fixing - colors are used to distinguish the VDs, and (c) joint estimation with aesthetic choice of gauge fixing.

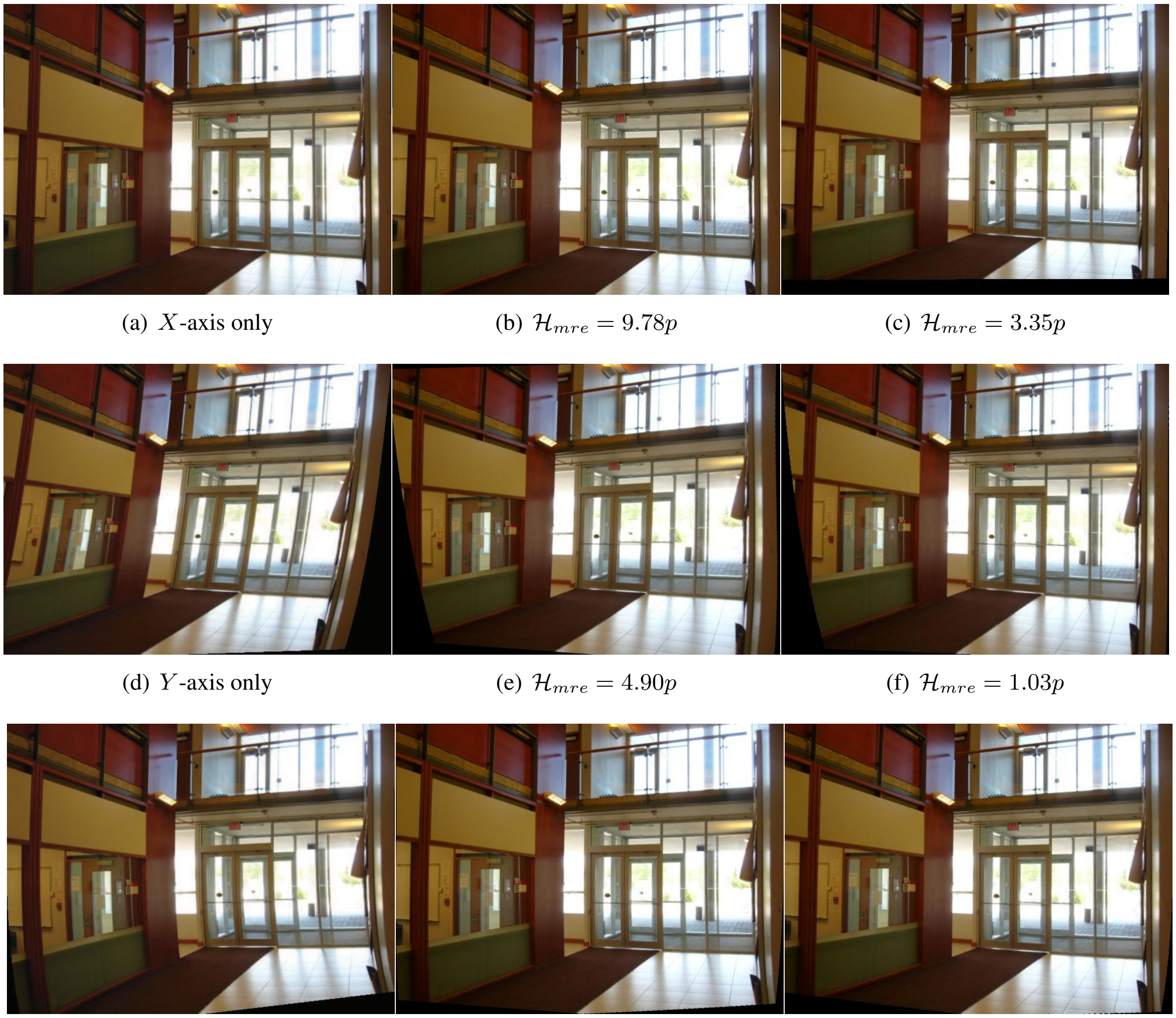

(a) X-axis only

(b) $\mathcal{H}_{mre} = 9.78p$

(c) $\mathcal{H}_{mre} = 3.35p$

(d) Y-axis only

(e) $\mathcal{H}_{mre} = 4.90p$

(f) $\mathcal{H}_{mre} = 1.03p$

(g) Z-axis only
Synthesized Image

(h) $\mathcal{H}_{mre} = 1.04p$
[26]

(i) $\mathcal{H}_{mre} = 0.70p$
[Ours]

Figure 8: Comparison of the proposed method with [26]: (a), (d) and (g) are the synthesized RS images where the motions are generated only along X-axis, Y-axis and Z-axis respectively. Images (b), (e) and (h) are the corresponding results by [26]. Images (e), (f) and (i) are the results by the proposed method. $\mathcal{H}_{mre}$ is the average error (in pixels) of the original image and restored image upto a global rotational homography.

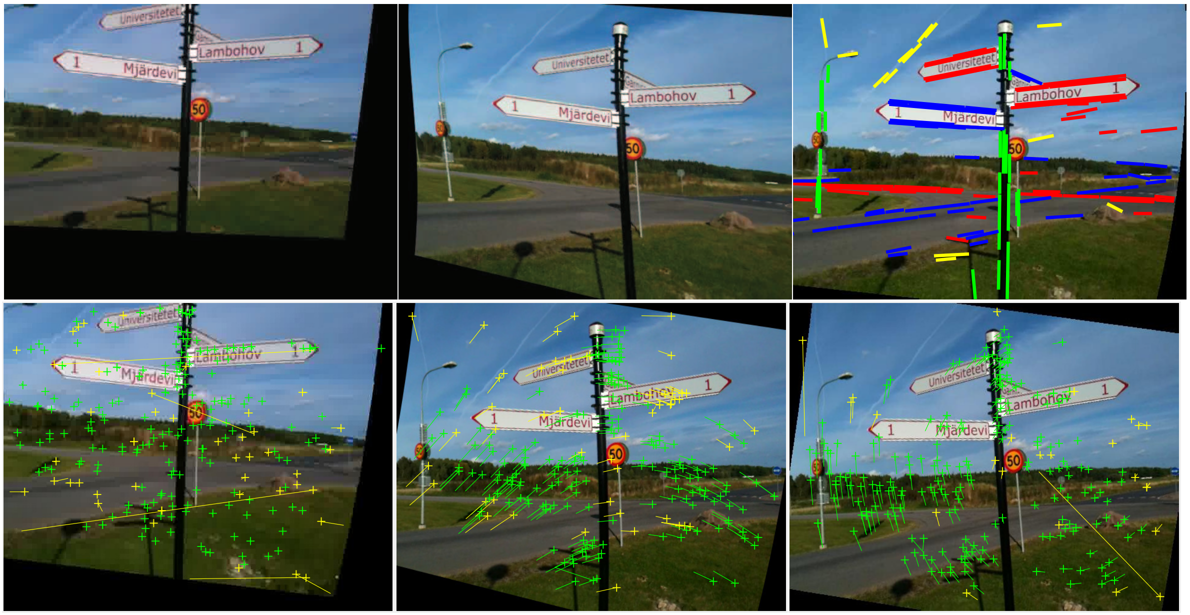

(a) $|\mathcal{R}_F| = 196.58, \sigma_{\mathcal{R}} = 7.60$ [9] (b) $|\mathcal{R}_F| = 186.44, \sigma_{\mathcal{R}} = 7.31$ [26] (c) $|\mathcal{R}_F| = 212.39, \sigma_{\mathcal{R}} = 8.40$ **[Ours]**

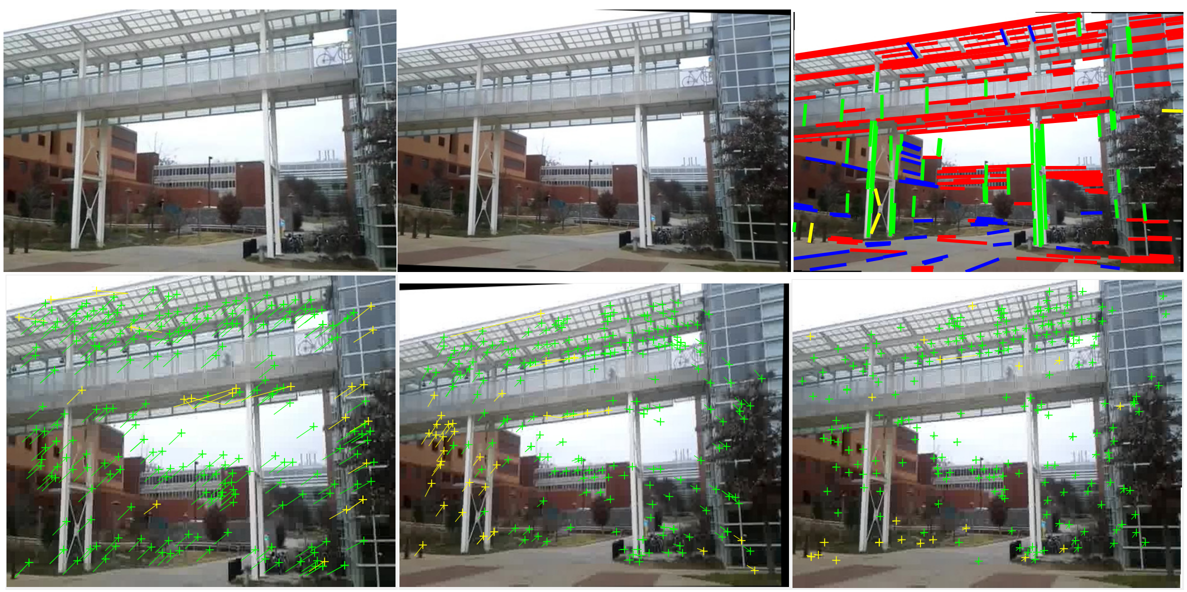

(d) $|\mathcal{R}_F| = 237.27, \sigma_{\mathcal{R}} = 3.49$ [12] (e) $|\mathcal{R}_F| = 229.44, \sigma_{\mathcal{R}} = 6.63$ [26] (f) $|\mathcal{R}_F| = 239.83, \sigma_{\mathcal{R}} = 4.94$ **[Ours]**

Figure 9: Comparison on the image sequences: (a)-(c) Results on `clip03.mov` sequence from [9] captured by an iPhone. (d)-(f) Results on `nxs_wobble_6_dual.mov` sequence from [12] captured by Nexus S. A selected image-pair from each of the sequences is displayed in separate rows for better qualitative comparison. The inliers-outliers are displayed only on the second image (bottom row) of the image pairs along with the mean and *std* of the number of inliers. The estimated VDs are also displayed.

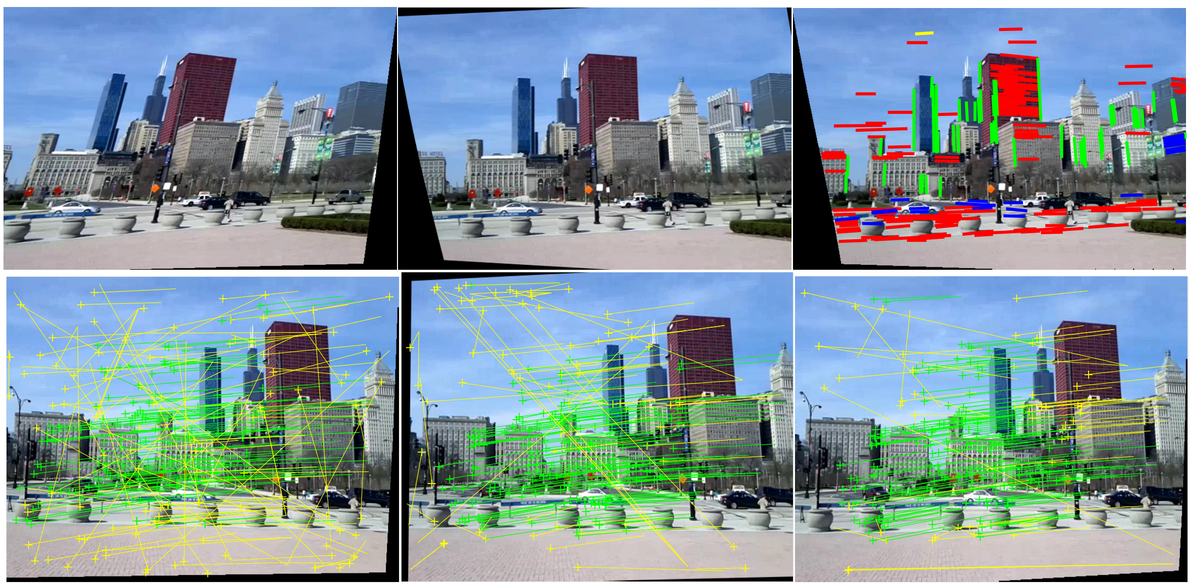

(a) $|\mathcal{R}_F| = 148.90$, $\sigma_{\mathcal{R}} = 2.47$ [16] (b) $|\mathcal{R}_F| = 196.44$, $\sigma_{\mathcal{R}} = 5.23$ [26] (c) $|\mathcal{R}_F| = 208.64$, $\sigma_{\mathcal{R}} = 5.67$ **[Ours]**

Figure 10: Comparison of the proposed method with [16] and [26] applied on a video sequence. We display the results on a image-pair of the sequence in separate rows, where inliers-outliers are displayed only on the second image.